Article

Homo sapiens and Neanderthals share high cerebral cortex integration into adulthood

🔴 Check for updates

Gabriele Sansalone ⬛ [1,2,11] ✉, Antonio Profico ⬛ [3,11] ✉, Stephen Wroe[1], Kari Allen[4], Justin Ledogar[5], Sarah Ledogar[1,6], Dave Rex Mitchell[7], Alessandro Mondanaro[8], Marina Melchionna[9], Silvia Castiglione[9], Carmela Serio ⬛ [10] & Pasquale Raia ⬛ [9]

There is controversy around the mechanisms that guided the change in brain shape during the evolution of modern humans. It has long been held that different cortical areas evolved independently from each other to develop their unique functional specializations. However, some recent studies suggest that high integration between different cortical areas could facilitate the emergence of equally extreme, highly specialized brain functions. Here, we analyse the evolution of brain shape in primates using three-dimensional geometric morphometrics of endocasts. We aim to determine, firstly, whether modern humans present unique developmental patterns of covariation between brain cortical areas; and secondly, whether hominins experienced unusually high rates of evolution in brain covariation as compared to other primates. On the basis of analyses including modern humans and other extant great apes at different developmental stages, we first demonstrate that, unlike our closest living relatives, *Homo sapiens* retain high levels of covariation between cortical areas into adulthood. Among the other great apes, high levels of covariation are only found in immature individuals. Secondly, at the macro-evolutionary level, our analysis of 400 endocasts, representing 148 extant primate species and 6 fossil hominins, shows that strong covariation between different areas of the brain in *H. sapiens* and *Homo neanderthalensis* evolved under distinctly higher evolutionary rates than in any other primate, suggesting that natural selection favoured a greatly integrated brain in both species. These results hold when extinct species are excluded and allometric effects are accounted for. Our findings demonstrate that high covariation in the brain may have played a critical role in the evolution of unique cognitive capacities and complex behaviours in both modern humans and Neanderthals.

The modern human brain is remarkable in its size, unusually globular shape and extreme left–right asymmetry, which are all thought to have contributed to the evolution of our exceptional cognitive capacities[1–5]. Historically, two main models have been invoked to explain the evolution of the brain: (1) the 'concerted' model, assuming that developmental integration affects brain evolution globally and (2)

the 'mosaic' model, that is the idea that functional units of the brain may co-evolve or evolve independently according to the distribution of selection pressures acting on them[6–9]. By deploying mosaicism, a brain module could be fine-tuned by selection to optimize specific tasks regardless of what happens in other areas of the brain[10–14]. Volumetric and morphometric analyses have demonstrated that selective
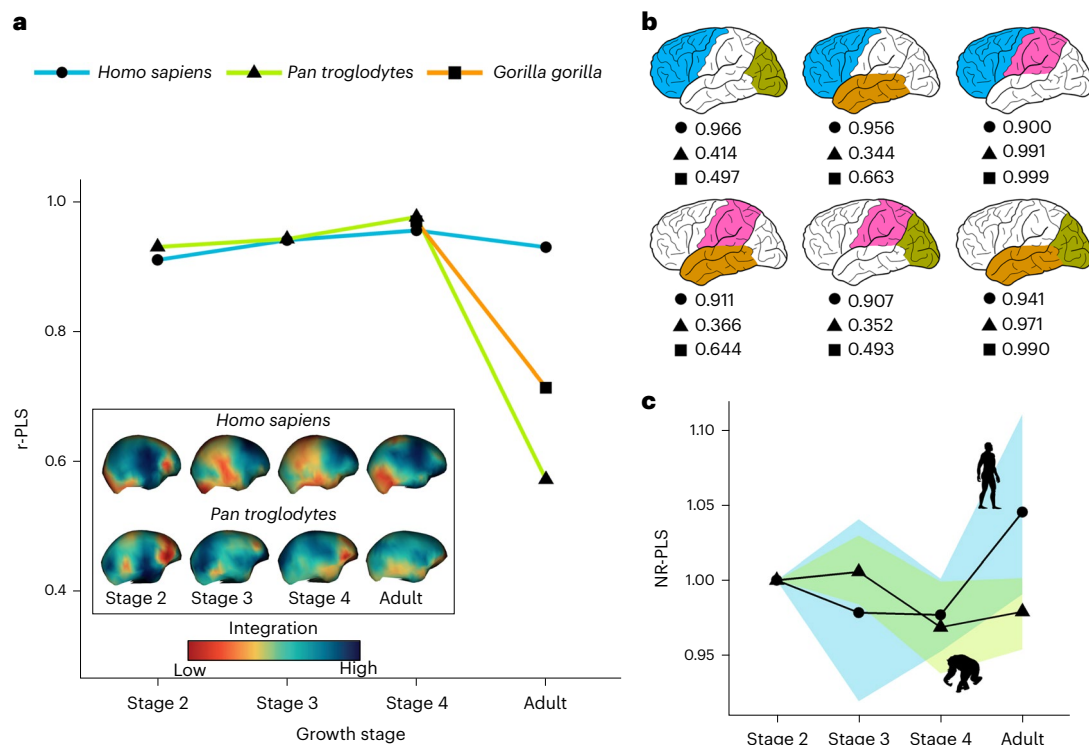
Fig. 1 | Patterns of postnatal integration in modern humans and chimpanzees. a, Postnatal growth stages for *H. sapiens*, *P. troglodytes*, *G. gorilla* (only stages 4 and adult) and r-PLS values per ontogenetic stage. The meshes in the lower left corner refer to the average for each stage and are coloured according to the magnitude of integration. **b**, Pairwise r-PLS values between brain modules in adult *H. sapiens*, *P. troglodytes* and *G. gorilla*. **c**, Comparison of r-PLS values per ontogenetic stage between *H. sapiens* and *P. troglodytes* calculated using the NR-PLS (r-PLS calculated between N-Core modulets and R-Core modules; see Methods) approach, that does not require the a priori definition of brain modules. Warm (cold) colours refer to low (high) magnitude of integration. Icons in **c** from PhyloPic.org under Creative Commons license CC BY 3.0.

expansion of discrete brain areas closely reflects the establishment of functional connections between them, enabling specific cognitive tasks[14–16]. It has also been proposed that mosaicism may have promoted behavioural flexibility and increased the ability to respond to changes in selective regimes[13]. However, the hypothesis of the brain modular evolution has been challenged by the recent observation that covariation of traits can favour the rapid evolution of extreme, highly specialized morphotypes, provided that selection vectors align with major axes of phenotypic variation[17,18]. Within this 'concerted' framework, it has been argued that the multiple, high-level functional specializations of the modern human brain could originate from selection for fine coordination between different brain units to shared functional ends, without effecting any major changes in the relative proportions of specific brain areas[10,19,20]. Despite their apparent polarization, the concerted and mosaic brain hypotheses are not mutually exclusive[16]. Mosaicism does not rule out covariation between brain units, as long as this reflects a response to shared functional demands, and a concerted brain can be the result of an adaptive process rather than the product of developmental constraints[21].

A key question regarding the uniqueness of the modern human brain is whether its evolution branched away from the developmental programme characterizing our living relatives. Studying the developmental patterns of morphological concertedness (or integration) as opposed to mosaicism (or modularity) between human brain areas and comparing this pattern to those of other great apes would help us determine to what extent the organization of cortical areas in *Homo sapiens* may actually be remarkable[1,22–25]. Another important issue is to understand whether, at the macro-evolutionary scale, humans display higher evolutionary rates toward either brain modularity or integration. This would offer direct evidence of selection favouring

the emergence of major changes in the patterns of covariation between cortical areas.

To address these questions, we have applied three-dimensional geometric morphometrics to measure and visualize the relative magnitudes of morphological covariation in primate virtual brain endocasts. Traditionally, investigations into patterns of covariation between different regions of the brain have relied on comparative volumetric analyses (of relative sizes) of brain subunits. However, volumetric comparisons are silent on the shape component (position and orientation) of brain form, which potentially captures aspects of brain evolution not predicted by size alone[13]. Furthermore, in contrast to volumetric data, shape data are comparatively rare for extinct species. Hence, studying patterns of covariation directly on cranial endocasts represents the single most informative means of gaining direct evidence on the evolutionary patterns of brain evolution across hominins (*H. sapiens* and its extinct close relatives). To gain this insight, we have combined a phylogenetic comparative method based on phylogenetic ridge regression to determine the presence of shifts in the evolutionary rates across primate history with a new strategy to measure and map phenotypic covariation on brain cortical areas. As brains do not fossilize, evidence of fossil species' brain evolution can be derived from the virtual fillings of the bony braincase—or endocasts—which can adequately approximate the outer brain morphology.

Our datasets comprise 127 postnatal virtual endocasts, sampled from the eruption of deciduous dentition through adulthood, for *H. sapiens*, *Pan troglodytes*, *Gorilla gorilla* and two species of *Pongo* for the analysis of developmental patterns; and, for the macro-evolutionary study 400 endocasts representing 154 extant and extinct species, including *Australopithecus africanus*, *Paranthropus boisei*, *Homo ergaster*, *Homo erectus*, *Homo heidelbergensis* and *Homo*
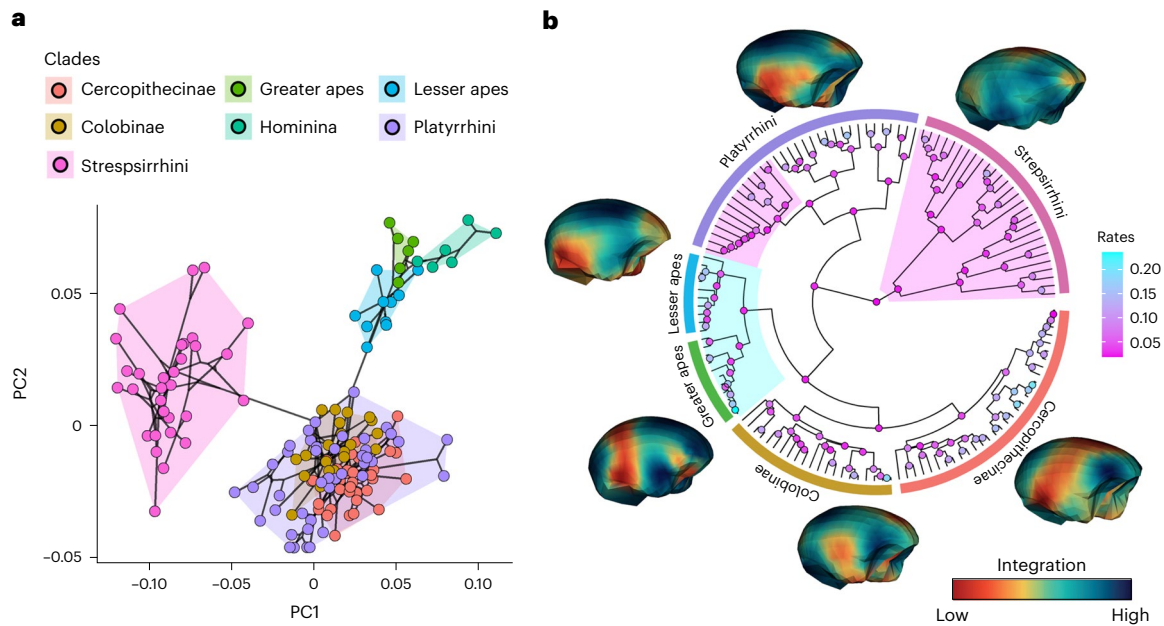
Fig. 2 | Macro-evolution of primate brain morphology and covariation. a, PC1/PC2 phylomorphospace of primate brain shape variation. **b**, Distribution of CR rate shifts on the tree. Magenta shades indicate a slowdown in CR rate of evolution, whereas the cyan shade indicates acceleration. Brain meshes represent the average shape for each clade and are coloured according to the magnitude of CR. Warmer colours refer to low CR values, cooler colours refer to high CR.

neanderthalensis. We explicitly tested whether: (1) specific patterns of modularity or integration between cortical areas can be identified through human brain development and how these relate to those of extant great apes; and (2) whether the hominin brain displays higher rates of evolution toward either increased integration or modularity.

Results

Does the human brain cortical covariation differ to that of other great apes?

We performed separate partial least squares (PLS) analyses on four successive postnatal developmental stages of *G. gorilla*, *P. troglodytes* and *H. sapiens*. We further included in the analysis *Pongo abelii* and *P. pygmaeus* (Fig. 1). Yet, given the paucity of available orangutan specimens we had to group them together and therefore did not explore covariation between individual brain modules in *Pongo*. The developmental stages were defined following refs. [26,27]: stage 2, all deciduous dentition fully erupted; stage 3, deciduous dentition and at least fully erupted M1; stage 4, M2 fully erupted; and adult, full permanent dentition. The PLS method allows the exploration of covariation patterns between different sets of shape variables (here, brain subunits), whereas r-PLS (measured using the r^2 derived from PLS analysis based on 999 permutations; Methods; Extended Data Tables 1 and 2 and Extended Data Fig. 1) is the correlation coefficient and can be used as a measure of the magnitude of covariation.

Our results show that integration of the brain in *H. sapiens* and *P. troglodytes* is similar through the pre-adult stages (stages 2 to 4; Fig. 1a and Extended Data Table 1). Yet, in chimpanzees (and in gorillas from stage 4 onwards), r-PLS significantly drops in adulthood, whereas in *H. sapiens* the brain remains significantly integrated into adulthood (Fig. 1 and Extended Data Table 1). The patterns of covariation between brain cortical modules are almost identical in adult *Pan* and *Gorilla* individuals, pointing to strong covariation between the occipital and temporal, and frontal and parietal modules, respectively (Fig. 1b). Comparable results are obtained when controlling for brain size (Extended Data Table 2) and whether *Pongo* species (grouped as one) are included. These results suggest that the shape covariation patterns observed

during development are largely independent from allometric effects and that humans significantly depart from the brain developmental patterns shared by the other greater apes.

Using two-block PLS to measure the degree of association between different cortical areas we confirmed the proposition that the brain of *H. sapiens* retains high levels of morphological integration throughout growth, unlike other great apes (Fig. 1b,c). We applied an approach to map the magnitude of morphological integration (Methods; Extended Data Fig. 1) directly onto the endocast surface without defining any a priori module. This approach involves parcelling out the brain endocasts into small independent 'modulets' centred around a single semilandmark and calculating the level of morphological integration of the modulets with the rest of the endocast. The average values of integration calculated at each semilandmark are subsequently used to create maps of integration intensity.

Charting the magnitude of integration over the endocasts at different developmental stages reveals clear differences between *H. sapiens* and *P. troglodytes* (Fig. 1a,c). At stage 2, the human brain displays high integration over the parietal and occipital regions. At stages 3 and 4, strong integration centres on the frontal and occipital lobes. In the adult stage (4), humans show the greatest level of integration over the parietal, temporal and prefrontal regions. Chimpanzees follow a different developmental pattern, showing poorly integrated frontal and parietal areas throughout postnatal growth and relatively stronger integration at the level of temporal and prefrontal areas.

Did hominins evolve towards high cortical integration?

We measured the covariation between four brain subunits (corresponding to frontal, parietal, temporal and occipital regions; Methods; Extended Data Table 3) at the macro-evolutionary level, by means of covariance ratio (CR; a measure of the overall covariation between modules divided by the overall covariation within modules; Methods).

Our results show that hominoid (apes) brains are morphologically distinct in shape (Fig. 2a) and display higher levels of covariation between brain cortical areas (CR = 1.01 indicating high covariation; Methods) than any other primate group (Fig. 2b and Extended
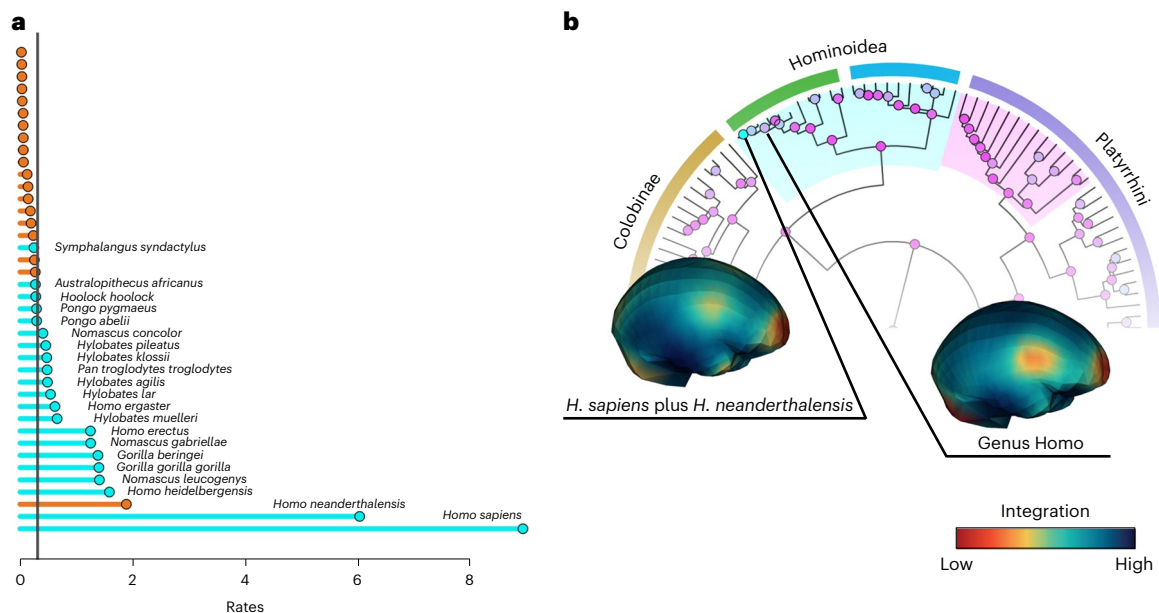
Fig. 3 | Evolutionary rates of integration within Hominoidea. a, Distribution of CR evolutionary rates within Hominoidea. The black vertical line represents the average rate of CR evolution calculated over the entire primate tree, orange dots indicate internal nodes in the phylogeny. *Australopithecus africanus* represents the Australopithecina subtribe. **b**, Evolutionary patterns of morphological integration within *Homo*. Magenta shades indicate a slowdown in the CR rate of evolution, the cyan shade indicates acceleration. Brain meshes represent the average shape for *H. sapiens* plus *H. neanderthalensis* and all *Homo* species, respectively. The CR values are mapped over the endocast mesh. Warmer colours refer to low CR values, cooler colours to high CR values.

Data Table 2; Methods). Platyrrhini and Strepsirrhini display the lowest magnitude of covariation (CR = 0.76 and 0.72, respectively) between brain modules, whereas Cercopithecinae and Colobinae fall in between hominoids and all other primates (CR = 0.83 and 0.91, respectively). Accounting for allometry did not alter the described pattern, suggesting that size has a limited impact on the brain covariation patterns observed at the macro-evolutionary level (Extended Data Table 3).

In keeping with our ontogenetic analyses, we devised an approach to map the metrics for the magnitude of covariation, the CR, over the digital endocasts. These brain maps show that hominins are characterized by the highest evolutionary rates in CR (Fig. 2b). Great apes display higher values of covariation in the occipital and parieto-frontal regions and lower levels over the temporal areas. In contrast, lesser apes show lower covariation in the prefrontal areas closer to the olfactory bulbs and over the temporal region (Fig. 2b).

Among Cercopithecinae, high evolutionary rates are recorded in Papionini (Fig. 2b and Extended Data Fig. 2). Conversely, Strepsirrhini (two-tailed *P* = 0.001) are characterized by a rate slowdown, as were capuchin and squirrel monkeys (family Cebidae, two-tailed *P* = 0.002) among New World monkeys (Fig. 2b and Extended Data Figs. 3 and 4). Mapping CR values over the endocast surfaces reveals different patterns in different primate clades. Cercopithecinae show higher integration in the occipital and frontal regions than elsewhere on the brain. Colobinae, Platyrrhini and Strepsirrhini display similar distribution of the CR values over the endocast, with the areas corresponding to the frontal and prefrontal cortical areas and the temporal regions showing moderate covariation (Fig. 2b).

Within Hominoidea, *H. neanderthalensis* and *H. sapiens* show the highest rate of evolution of brain covariation (two-tailed *P* = 1.00, Fig. 3). Interestingly, Australopithecina (*A. africanus* + *P. boisei*, grouped as one) was characterized by evolutionary rates comparable to those of *P. troglodytes* suggesting a graded trend for increased rate of CR evolution among hominins (Fig. 3a), leading to the highly integrated brain of *Homo*, especially evident in the parietal area (Fig. 3b).

Discussion

H. sapiens and the other great apes share high covariation between different cortical areas of the brain throughout most postnatal development. However, only *H. sapiens* retains such strong morphological integration into adulthood. This finding is consistent with other reports indicating that the cortical areas of the human brain are tightly integrated throughout the adult life[12,28]. Connectome analysis suggests an evolutionary shift in the human brain to enhance global network integration over that of the chimpanzee[29], indicating that humans evolved strong covariation even among spatially distant brain regions[30] (which is consistent with our Fig. 1c). This evolutionary pattern seems to have deep evolutionary roots. Hominins show a trend for an increased magnitude of covariation between different brain regions, escalating through Middle to Late Pleistocene human species (*H. sapiens* and *H. neanderthalensis*). This finding contradicts the common perception that functional specialization in the modern human brain arises from a modular architecture (for example, semi-independent evolution of different cortical areas)[13] but is in agreement with studies of encephalized non-mammalian vertebrates suggesting that high integration may drive functional specialization in the brain, even among distantly related taxa and under very different selective scenarios[31]. Our findings similarly suggest that coordinated changes in brain shape may have played a major role in maintaining the functional association between brain subunits, ultimately leading to the derived cognitive specialization observed in *Homo*.

Charting morphological integration over the endocasts shows that the great apes are clearly distinct from the lesser apes, suggesting that a shift in the spatial patterns of covariation (and not just in the magnitude of integration or relative brain size) occurred at the time of divergence between the two groups. Hominins show a high degree of covariation in the parietal and frontal regions, which are thought to have played a fundamental role in the evolution of cognitive capacities unique to humans[32,33]. Modifications in the parietal regions are thought to represent a derived condition apparent only within the most recent *H. sapiens* populations[23,34]. The parietal cortex is involved in different

association tasks such as dexterity, self-awareness and visual imaging[35]. These functions confer the capacity to translate cognition into new behavioural attributes, allowing the incorporation of tools and technology into behavioural patterns[33,36].

Australopithecina, *H. ergaster* and *H. erectus* display evolutionary rates like, or slightly higher than, those showed by *P. troglodytes* and *P. paniscus* (Fig. 3a). In general, larger-bodied species, mostly occurring among hominoids and papionins, are marked by higher rates of covariation among brain areas[37]. Yet, even after correcting for brain size, the *Homo* clade still shows the highest levels and rates of brain cortex covariation (Extended Data Table 3). This suggests that the major shift in the pattern of brain shape covariation emerged independently from size and, probably, occurred within these species only. This increased level of interconnection between different cortical areas of the brain may have facilitated the emergence of derived cognitive capacities in Neanderthals as suggested by the palaeoanthropological record[38-41]. However, modern humans and Neanderthals have distinctly different brain morphologies, suggesting that high levels of covariation might have been inherited from their last common ancestor and that brain shape evolution then followed divergent trajectories in *H. neanderthalensis* and *H. sapiens*[42]. This evidence brings into question the role of globularity in the emergence of high cognitive abilities in *H. sapiens*. Neanderthals and the other great apes, did not go through a 'globularization phase' during the earliest postnatal growth stages, retaining the plesiomorphic, anteroposteriorly elongated adult brain common to archaic *Homo* species[43,44]. The development of a globular brain is exclusive to modern humans[45] and its role in maintaining high levels of integration into adulthood deserves further investigation.

Our findings do not favour either the mosaic or the concerted model of brain evolution, suggesting that the debate between these two hypotheses of brain evolution should be reframed within a more inclusive proposition. We found that a shared or conserved pattern of covariation could have an adaptive value or be instrumental to the emergence of derived modern humans functional capacities, rather than being considered a mere developmental or phylogenetic constraint[21]. In contrast, this study suggests that departure from an established pattern does not necessarily involve the presence of a modular behaviour and that high covariation may favour the emergence of functional specialization, as predicted by the mosaic model.

In conclusion, we propose that the persistence of high levels of morphological covariation into adulthood in modern humans and Neanderthals is linked to the evolution of derived cognitive abilities. In addition, modern humans show high levels of integration between cortical areas throughout development. Unfortunately, the scarcity of immature Neanderthals with well-preserved skulls prohibits us from conclusively determining whether the *H. neanderthalensis* brain followed the same developmental path as ours[43,44]. Yet, the strong covariation in adult brains shared by Neanderthals and *H. sapiens* only, suggests this is arguably the case.

Neural plasticity and innovative–explorative behaviours are typically associated with juvenile life stages, as well as the extension of childhood learning[45,46] and are central to Mithen's theory of cognitive fluidity[47,48], which postulates that only modern humans are capable of fully integrating diverse dominions of knowledge. Our evidence supports the argument that juvenilization of the human brain (and possibly to some extent the Neanderthal brain) was driven by prolonged brain growth, mediated by the retention of an unusually high degree of covariation between the different brain units into adulthood.

Methods

Endocast segmentation
Virtual endocasts of primate crania were generated from computed tomography image stacks using a combination of Materialise Mimics 21.0 and Geomagic Studio 2014. For each specimen, cranial bone was first segmented in Mimics with the grey-value range set conservatively to avoid extensive manual corrections later in the process. The endocranial cavity was then closed off at the foramen magnum using a flat plane spanning basion to opisthion. Next, a three-dimensional object was generated and all gaps <1 mm in diameter were closed using the Wrap function before closing off all remaining openings (for example, foramen ovale and optic canal) near the endocranial surface. This created a sealed cavity that was filled using the Cavity Fill tool. Endocasts were then imported as stereolithography-formatted surface files into Geomagic where excess material protruding through cranial foramina was removed and the polygon meshes were lightly smoothed using the QuickSmooth function. Endocast volumes were then measured in cm^3 using the Compute Volume function.

Automatic landmarking procedure
The points on the template (*Piliocolobus badius*) were projected on all the other specimens using the function placePatch() from the R package Morpho[49]. To remove any incorrect projection the semilandmarks on the curves were set bold-distanced using the function pointsOnBezier() from the bezier R package[50] then the curves present on the sides of the endocast geometry were mirrored using the function symmetrize() from the R package Morpho. After this process was complete, the semilandmarks were slid along the curves by minimizing the bending energy of a thin plate spine deformation (semilandmarks relaxation) using the slider3d() function from the R package Morpho. This approach follows the algorithm described by ref. [51] and has been shown to be the most appropriate method to slide semilandmarks on curves and surfaces according to ref. [52].

Shape analysis
On each endocast (Supplementary Fig. 1), we manually digitized 21 anatomical and homologous landmarks, then performed a principal component analysis (PCA) to identify the individual closest to the consensus shape (*P. badius* USNM 481795). We manually digitized 76 semilandmarks placed equidistantly along curves and surfaces on the consensus specimen endocast and used it as the template individual (Supplementary Table 1). All landmarks were placed by using IDAV Landmark software. Once all the semilandmarks were automatically placed, we imported the landmark coordinates into R v.4.0.1 for further analyses. We performed generalized Procrustes analysis (GPA) on all landmarks, implemented in the function procSym from the R package Morpho to rotate, translate and scale landmark configurations to unit centroid size, that is the square root of squared differences between landmark coordinates and centroid coordinates[53]. To visualize the multivariate ordination of the aligned Procrustes coordinates, we used a phylomorphospace using the first two regular non-phylogenetic PCA scores. We classified the species using similar taxonomic groups to those defined in refs. [4,54]: Hominoidea, Cercopithecinae, Colobinae, Platyrrhini and Strepsirrhini. Shape data have been controlled for size (Extended Data Tables 2 and 3), sexual dimorphism effects and for measurement error.

Phylogeny
The phylogenetic tree used in our analyses is a time-calibrated tree based on a Bayesian estimate obtained from the 10kTrees Project v.3 (ref. [55]) for the 146 extant species in our dataset. A maximum clade credibility tree of the extant species in the analysis was constructed from a set of 1,000 molecular trees using the function MaxCredTree() from the R package phangorn[56]. Finally, the eight fossil species included in our dataset were manually added to the tree (available in Newick format in the Supplementary Information) following the topological arrangement in refs. [2,57,58] using the RRphylo function tree.merger[59]. The full list of the accessed specimens is indicated in Supplementary Table 2.

Measurement error
The measurement error associated with the digitization of landmarks was measured on three replicates of 60 specimens representative of

the total dataset variation. For each specimen we digitized only the homologous landmarks; subsequently we automatically applied the semilandmarks following the procedure previously described. We calculated the mean Procrustes distances for each triplet of the same specimen occurring in the three replicas. We then computed the averages of all the mean values of the minimum and maximum values of each triplet. The amount of digitization error, with respect to the total variation in the shape, can be expressed as a percentage. We calculated the ratio of the mean value for total digitization and the mean of the total dataset. We found the digitization error in the endocast dataset was as low as 0.36% of the total variation, respectively. Because the measurement error was smaller than 5% in both datasets it could be safely assumed that its effect on the results was negligible.

Sexual dimorphism

To account for the potential effect of sexual dimorphism on the shape data, we performed a Procrustes analysis of variance to test for the presence of significant shape and size differences between males and females. The analysis returned a non-significant result ($r^2 = 0.01$, $P = 0.28$), suggesting that, at macro-evolutionary scale, sexual dimorphism is not impacting the brain shape variation in primates. Similar results were obtained when we tested for size differences between males and females ($r^2 = 0.01$, $P = 0.24$).

Size and phylogenetic correction

The relationship between size (measured as centroid size; independent variable) and shape (measured as aligned Procrustes coordinates; dependent variable) was tested by means of multivariate regressions. We repeated all the following analyses by using residuals of the multivariate regression of shape versus size.

Specifically, to account for size effects on the ontogenetic series, we used shape residuals computed from separate, per developmental stage, multivariate regression. The shape residuals were used to perform size-free PLS analyses and the results are summarized in Extended Data Table 2. Overall, we did not observe any difference from the pattern described by the standard version of the PLS. However, it must be noted the r-PLS were lower for each group. This is in agreement with previous findings reporting allometry and development as integrating factors, therefore the removal of the size component may reduce the observed levels of covariation[60].

The same holds for the macro-evolutionary analyses, which we repeated using residuals of multivariate regressions of shape versus size performed within a phylogenetic context using phylogenetic generalized least squares (PGLS) regression. Specifically, shape residuals have been computed using the function PGLS_fossil() from the R package RRphylo. It must be noted that the PGLS analysis using shape as the respondent and size as the predictor variables and accounting for phylogenetic variance covariance matrix, returned marginally significant results ($P = 0.042$, $r^2 = 0.101$) suggesting that size is explaining a relatively small fraction of the total shape variation; this result is in line with previous investigations indicating a limited effect of size on primates' brain shape[4,22].

We computed the CR (more details below) values using shape residuals (results are summarized in Extended Data Table 3) for the different primate clades while accounting for phylogeny using the function phylo.modularity() from the R package geomorph. Furthermore, we used shape residuals to compute per-species CR values to then compute size-free evolutionary rates of covariation. Again, we did not notice any alteration in the pattern produced by the standard RRphylo analyses of evolutionary rates, with the major shifts identified on the same nodes.

Assessing brain covariation

We measured the magnitude of covariation between the different ontogenetic stages by using the standard PLS analysis. PLS differs from linear regression by treating the two variables symmetrically rather than using one set of variables (independent) to predict the other. Instead, PLS constructs new variables that are linear combinations of the variables within each of the sets, accounting for as much as possible of the covariation between the two original sets of variables.

The magnitude of morphological covariation in the brain at the macro-evolutionary context has been assessed using the CR coefficient measured accounting for shared ancestry applying the function phylo. modularity from the R package geomorph[61]. The CR coefficient is a measure of the overall covariation between modules divided by the overall covariation within modules. The CR coefficient ranges from 0 to positive values, where lower values indicate low covariation and high values indicate higher covariation; here, departure from the null hypothesis of random association between modules is assessed via permutation. Furthermore, measuring the CR coefficient is insensitive to variation in sample size and number of variables as the variance of each module is not included. These analyses were repeated after accounting for the effect of size measured as logarithm of centroid size.

Finally, it has been recently noted[62] that sliding semilandmarks using the minimum bending energy (BEN) approach may result in increased covariation between modules. Because we used semilandmarks in our dataset, we repeated all the following integration analyses using shape coordinates derived using both the minimum BEN and minimum Procrustes distances approaches to evaluate any potential discrepancy in the results. We found no significant discrepancies when using either sliding methods, hence we present only the results obtained from the analyses performed on the shape coordinates derived after using the minimum BEN approach.

Assessing endocast modular partitioning

Brain covariation was measured by dividing the brain into six distinct subunits following previously published protocols and on the recognition of traits on the cortical surface areas identified from the three-dimensional reconstruction[2,4,23,35,63–65] (Supplementary Fig. 2). (1 and 2) The frontal and prefrontal regions extend from the frontal pole anteriorly to the central sulcus posteriorly. The central sulcus is a longitudinal unfolding beginning on the medial surface of the brain. The frontal region borders with the postcentral gyrus of parietal lobe and it is separated from the temporal lobe by the lateral sulcus[66]. (3) The anterior border of the parietal region is demarcated by the central sulcus and the inferior border is demarcated by the Sylvian fissure. It extends posteriorly where it meets the occipital areas. (4) The parietal lobe can be further subdivided into major subareas which can be identified from the endocranial surface (supramarginal gyrus, angular gyrus, intraparietal sulcus and superior parietal lobule)[65]. (5) The temporal lobe is separated from the other cortical area by the Sylvian fissure, a feature unique to primates[67]. (6) The occipital lobe is the most posterior region of the brain and borders the parieto-occipital fissure which separates it from the parietal areas[68].

However, describing different modules on the endocasts can be challenging and to better define the different regions we accounted for the uncertainties of assessing clear boundaries between the different modules by using two different strategies.

(1) We defined four different modular configurations and evaluate between them by using the standardized test statistics based on the comparison of the CR measurement. This assesses the covariances within and among hypothesized modules and compares this ratio with a null hypothesis of random assignment of shape variables to partitions[69,70]. We found that the most supported configuration was the one formed by four distinct modules (Supplementary Fig. 2 and Supplementary Table 3).

(2) We devised a strategy to measure the intensity of local modularity and integration without defining modules a priori. In geometric morphometrics applications, a module is defined

as a discrete region characterized by greater integration internally than externally. To locate brain areas matching this condition, for each semilandmark we selected its nine closest semilandmarks, forming a candidate modulet (N-Core) of ten semilandmarks. All the other semilandmarks of the entire set define a second module (R-Core) (Extended Data Fig. 1). We calculated the CR between N-Core and R-Core, repeated the operation over all semilandmarks for the entire set and mapped CR values on a reference mesh. The CR between each N-Core and its corresponding R-Core indicated how much N-Core is likely to form a discrete module (Supplementary Figs. 3 and 4).

A similar procedure was used to calculate the local integration by computing the correlation of the first PLS axis between N-Cores and R-Cores. At each iteration, the GPA is performed separately on each of the two blocks (N- and R-Cores). This way, by using PLS the level of integration was calculated iteratively over all semilandmarks of the entire sample.

RRphylo and overfitRR

We derived rates of brain shape evolution by the RRphylo method[71], available within the R package RRphylo (v.2.5.0). Under RRphylo, consequent phenotypic changes occurring along a phyletic line, from the root to a species are given by the equation $\Delta P = \beta_1 l_1 + \beta_2 l_2 + \ldots + \beta_n l_n$ where β_{ith} and l_{ith} represent the regression coefficient and branch length, respectively, for each ith branch along the phyletic line. Being regression slopes, the β coefficients represent the magnitude of phenotypic change occurring along each branch; that is, the actual rate of phenotypic evolution. The matrix solution to find the vector of β coefficients for all the branches is given by the equation $\hat{\beta} = (L^T L + \lambda I)^{-1} L^T \mathbf{y}$; where L is the matrix of species to root time distances of the tree (the branch lengths), having tips as rows, $\mathbf{y}$ is the vector of species phenotypes and $\hat{\beta}$ is the vector of rates. The λ is a penalization factor which prevents overfitting by penalizing extremely large rates. Factor λ is derived by means of maximum likelihood estimation by minimizing rate variance within clades as compared to variance between clades.

To locate clade-wise shifts in evolutionary rates, we used the function search.shift from the package RRphylo[71]. Function search.shift is specifically meant to automatically scan the phylogeny to identify shifts in absolute phenotypic evolutionary rates. Given rates as produced by RRphylo, search.shift starts by selecting all the subclades within the tree ranging from one-tenth to one-half of the total tree size. For each clade, it computes the difference between the mean absolute rate pertaining the branches within the clade and the same figure for all other branches within the tree. Each difference is compared to a random distribution of 1,000 differences derived by randomly swapping rate values among the branches.

To account for sampling, phylogenetic uncertainty in tree topology and branch lengths, we used the RRphylo function overfitRR. Over 100 consecutive iterations, the function randomly removes a number of tips corresponding to 25% of the tree size and swaps species phylogenetic position of the 10% of the remaining species. For instance, a topology of the kind ((A, B), C) might change to ((C, B), A) or ((A, C), B). In addition, the age of 10% of the tree nodes is changed 'moving' the node in between the age of its direct ancestor and the age of its oldest daughter node. At each iteration, overfitRR performs search.shift on pruned tree and data testing whether the pattern found with the original data is robust to sampling and phylogenetic uncertainty issues. The results of the analysis of rates of CR evolution were confirmed, after accounting for phylogenetic uncertainty, by randomly swapping tree branches and node ages, suggesting that they are not a consequence of the tree topology we used (Hominoidea, $P = 0.99$; Strepsirrhini, $P = 0.01$; Cebidae, $P = 0.01$).

References

1. Ponce de León, M. S. et al. The primitive brain of early *Homo*. *Science* **372**, 165–171 (2021).
2. Melchionna, M. et al. From smart apes to human brain boxes. A uniquely derived brain shape in late hominins clade. *Front. Earth Sci.* **8**, 273 (2020).
3. Du, A. et al. Pattern and process in hominin brain size evolution are scale-dependent. *Proc. R. Soc. B* **285**, 20172738 (2018).
4. Sansalone, G. et al. Variation in the strength of allometry drives rates of evolution in primate brain shape. *Proc. R. Soc. B* **287**, 20200807 (2020).
5. Gunz, P. et al. Neanderthal introgression sheds light on modern human endocranial globularity. *Curr. Biol.* **29**, 120–127 (2019).
6. Finlay, B. L. & Darlington, R. B. Linked regularities in the development and evolution of mammalian brains. *Science* **268**, 1578–1584 (1995).
7. Barton, R. A. & Harvey, P. H. Mosaic evolution of brain structure in mammals. *Nature* **405**, 1055–1058 (2000).
8. Harvey, P. H. & Krebs, J. R. Comparing brains. *Science* **249**, 140–146 (1990).
9. Finlay, B. L., Darlington, R. B. & Nicastro, N. Developmental structure in brain evolution. *Behav. Brain Sci.* **24**, 263–278 (2001).
10. Barton, R. A. & Venditti, C. Human frontal lobes are not relatively large. *Proc. Natl Acad. Sci. USA* **110**, 9001–9006 (2013).
11. Barton, R. A. & Venditti, C. Rapid evolution of the cerebellum in humans and other great apes. *Curr. Biol.* **24**, 2440–2444 (2014).
12. Sotiras, A. et al. Patterns of coordinated cortical remodeling during adolescence and their associations with functional specialization and evolutionary expansion. *Proc. Natl Acad. Sci. USA* **114**, 3527–3532 (2017).
13. Gómez-Robles, A., Hopkins, W. D. & Sherwood, C. C. Modular structure facilitates mosaic evolution of the brain in chimpanzees and humans. *Nat. Commun.* **5**, 4469 (2014).
14. Smaers, J. B. & Vanier, D. R. Brain size expansion in primates and humans is explained by a selective modular expansion of the cortico-cerebellar system. *Cortex* **118**, 292–305 (2019).
15. DeCasien, A. R. & Higham, J. P. Primate mosaic brain evolution reflects selection on sensory and cognitive specialization. *Nat. Ecol. Evol.* **3**, 1483–1493 (2019).
16. Montgomery, S. H., Mundy, N. I. & Barton, R. A. Brain evolution and development: adaptation, allometry and constraint. *Proc. R. Soc. B* **283**, 20160433 (2016).
17. Villmoare, B. Morphological integration, evolutionary constraints, and extinction: a computer simulation-based study. *Evol. Biol.* **40**, 76–83 (2013).
18. Goswami, A., Smaers, J. B., Soligo, C. & Polly, P. D. The macroevolutionary consequences of phenotypic integration: from development to deep time. *Philos. Trans. R. Soc. B* **369**, 20130254 (2014).
19. Herculano-Houzel, S. The remarkable, yet not extraordinary, human brain as a scaled-up primate brain and its associated cost. *Proc. Natl Acad. Sci. USA* **109**, 10661–10668 (2012).

20. Barton, R. A. & Montgomery, S. H. Proportional versus relative size as metrics in human brain evolution. *Proc. Natl Acad. Sci. USA* **116**, 3–4 (2019).

21. Avin, S., Currie, A. & Montgomery, S. H. An agent-based model clarifies the importance of functional and developmental integration in shaping brain evolution. *BMC Biol.* **19**, 97 (2021).

22. Aristide, L. et al. Brain shape convergence in the adaptive radiation of New World monkeys. *Proc. Natl Acad. Sci. USA* **113**, 2158–2163 (2016).

23. Neubauer, S., Hublin, J.-J. & Gunz, P. The evolution of modern human brain shape. *Sci. Adv.* **4**, eaao5961 (2018).

24. Neubauer, S., Gunz, P., Scott, N. A., Hublin, J. J. & Mitteroecker, P. Evolution of brain lateralization: a shared hominid pattern of endocranial asymmetry is much more variable in humans than in great apes. *Sci. Adv.* **6**, eaax9935 (2020).

25. Ni, X., Flynn, J. J., Wyss, A. R. & Zhang, C. Cranial endocast of a stem platyrrhine primate and ancestral brain conditions in anthropoids. *Sci. Adv.* **5**, eaav7913 (2019).

26. Cobb, S. N. & O'Higgins, P. The ontogeny of sexual dimorphism in the facial skeleton of the African apes. *J. Hum. Evol.* **53**, 176–190 (2007).

27. Ragni, A. J. Trabecular architecture of the capitate and third metacarpal through ontogeny in chimpanzees (*Pan troglodytes*) and gorillas (*Gorilla gorilla*). *J. Hum. Evol.* **138**, 102702 (2020).

28. Nadig, A. et al. Morphological integration of the human brain across adolescence and adulthood. *Proc. Natl Acad. Sci. USA* **118**, e2023860118 (2021).

29. Ardesch, D. J. et al. Evolutionary expansion of connectivity between multimodal association areas in the human brain compared with chimpanzees. *Proc. Natl Acad. Sci. USA* **116**, 7101–7106 (2019).

30. Garin, C. M. et al. An evolutionary gap in primate default mode network organization. *Cell Rep.* **39**, 110669 (2022).

31. Watanabe, A., Balanoff, A. M., Gignac, P. M., Gold, M. E. L. & Norell, M. A. Novel neuroanatomical integration and scaling define avian brain shape evolution and development. *eLife* **10**, e68809 (2021).

32. Stout, D. & Chaminade, T. Stone tools, language and the brain in human evolution. *Philos. Trans. R. Soc. B* **367**, 75–87 (2012).

33. Bruner, E. & Iriki, A. Extending mind, visuospatial integration, and the evolution of the parietal lobes in the human genus. *Quat. Int.* **405**, 98–110 (2016).

34. Schaefer, N. K., Shapiro, B. & Green, R. E. An ancestral recombination graph of human, Neanderthal, and Denisovan genomes. *Sci. Adv.* **7**, 776–792 (2021).

35. Bruner, E., Spinapolice, E., Burke, A. & Overmann, K. A. in *Evolution of Primate Social Cognition* (eds Di Paolo, L. E. et al.) 299–326 (Springer, 2018).

36. Bruner, E. & Gleeson, B. T. Body cognition and self-domestication in human evolution. *Front. Psychol.* **10**, 1111 (2019).

37. Porto, A., de Oliveira, F. B., Shirai, L. T., de Conto, V. & Marroig, G. The evolution of modularity in the mammalian skull I: morphological integration patterns and magnitudes. *Evol. Biol.* **36**, 118–135 (2009).

38. Conde-Valverde, M. et al. Neanderthals and *Homo sapiens* had similar auditory and speech capacities. *Nat. Ecol. Evol.* **5**, 609–615 (2021).

39. Hardy, B. L. et al. Direct evidence of Neanderthal fibre technology and its cognitive and behavioral implications. *Sci. Rep.* **10**, 4889 (2020).

40. Mondanaro, A. et al. A major change in rate of climate niche envelope evolution during hominid history. *iScience* **23**, 101693 (2020).

41. Leder, D. et al. A 51,000-year-old engraved bone reveals Neanderthals' capacity for symbolic behaviour. *Nat. Ecol. Evol.* **5**, 1273–1282 (2021).

42. Hublin, J. J., Neubauer, S. & Gunz, P. Brain ontogeny and life history in pleistocene hominins. *Philos. Trans. R. Soc. B* **370**, 20140062 (2015).

43. Gunz, P., Neubauer, S., Maureille, B. & Hublin, J. J. Brain development after birth differs between Neanderthals and modern humans. *Curr. Biol.* **20**, R921–R922 (2010).

44. Gunz, P. et al. A uniquely modern human pattern of endocranial development. insights from a new cranial reconstruction of the Neandertal newborn from Mezmaiskaya. *J. Hum. Evol.* **62**, 300–313 (2012).

45. Gunz, P. et al. *Australopithecus afarensis* endocasts suggest ape-like brain organization and prolonged brain growth. *Sci. Adv.* **6**, eaaz4729 (2020).

46. Pellegrini, A. D., Dupuis, D. & Smith, P. K. Play in evolution and development. *Dev. Rev.* **27**, 261–276 (2007).

47. Mithen, S. The prehistory of the mind. *Camb. Archaeol. J.* **7**, 269 (1997).

48. Mithen, S. *Creativity in Human Evolution and Prehistory* (Routledge, 2005).

49. Schlager, S. in *Statistical Shape and Deformation Analysis: Methods, Implementation and Applications* (eds Zheng, G. et al.) 217–256 (2017).

50. Olsen, A. bezier: Toolkit for Bezier curves and splines. R package version 1.1.2 (2018).

51. Gunz, P., Mitteroecker, P. & Bookstein, F. L. in *Modern Morphometrics in Physical Anthropology* (ed. Slice, D. E.) 73–98 (Kluwer Academic Publishers-Plenum Publishers, 2006).

52. Bookstein, F. L. Integration, disintegration, and self-similarity: characterizing the scales of shape variation in landmark data. *Evol. Biol.* **42**, 395–426 (2015).

53. Bookstein, F. L. in *Biennial International Conference on Information Processing in Medical Imaging* (eds Colchester, A. C. F. & Hawkes, D. J.) 326–342 (Springer, 1991).

54. Neaux, D. et al. Basicranium and face: assessing the impact of morphological integration on primate evolution. *J. Hum. Evol.* **118**, 43–55 (2018).

55. Arnold, C., Matthews, L. J. & Nunn, C. L. The 10kTrees website: a new online resource for primate phylogeny. *Evol. Anthropol.* **19**, 114–118 (2010).

56. Schliep, K.P phangorn: phylogenetic analysis in R. *Bioinformatics* **27**, 592–593 (2011).

57. Dembo, M., Matzke, N. J., Mooers, A. Ø. & Collard, M. Bayesian analysis of a morphological supermatrix sheds light on controversial fossil hominin relationships. *Proc. R. Soc. B* **282**, 20150943 (2015).

58. Organ, C., Nunn, C. L., Machanda, Z. & Wrangham, R. W. Phylogenetic rate shifts in feeding time during the evolution of *Homo. Proc. Natl Acad. Sci. USA* **108**, 14555–14559 (2011).

59. Castiglione, S., Serio, C., Mondanaro, A., Melchionna, M. & Raia, P. Fast production of large, time-calibrated, informal supertrees with tree.merger. *Palaeontology* **65**, e12588 (2022).

60. Machado, F. A., Hubbe, A., Melo, D., Porto, A. & Marroig, G. Measuring the magnitude of morphological integration: the effect of differences in morphometric representations and the inclusion of size. *Evolution* **73**, 2518–2528 (2019).

61. Adams, D. C. & Otárola-Castillo, E. geomorph: an R package for the collection and analysis of geometric morphometric shape data. *Methods Ecol. Evol.* **4**, 393–399 (2013).

62. Cardini, A. Integration and modularity in Procrustes shape data: is there a risk of spurious results? *Evol. Biol.* **46**, 90–105 (2019).

63. Neubauer, S., Gunz, P. & Hublin, J. J. The pattern of endocranial ontogenetic shape changes in humans. *J. Anat.* **215**, 240–255 (2009).

64. Wild, H. M., Heckemann, R. A., Studholme, C. & Hammers, A. Gyri of the human parietal lobe: volumes, spatial extents, automatic labelling, and probabilistic atlases. *PLoS ONE* **12**, e0180866 (2017).

65. Pereira-Pedro, A. S., Bruner, E., Gunz, P. & Neubauer, S. A morphometric comparison of the parietal lobe in modern humans and Neanderthals. *J. Hum. Evol.* **142**, 102770 (2020).

66. Parks, A. N. & Smaers, J. B. in *Digital Endocasts: From Skulls to Brains* (eds Bruner, E. et al.) 205–218 (Springer, 2018).

67. Preuss, T. M. in *Primate Origins: Adaptations and Evolution* (eds Ravosa, M. J. & Marian Dagosto, M.) 625–675 (Springer, 2007).

68. Todorov, O. S. & de Sousa, A. A. in *Digital Endocasts: From Skulls to Brains* (eds Bruner, E. et al.) 259–273 (Springer, 2018).

69. Adams, D. C. & Collyer, M. L. Comparing the strength of modular signal, and evaluating alternative modular hypotheses, using covariance ratio effect sizes with morphometric data. *Evolution* **73**, 2352–2367 (2019).

70. Adams, D. C. Evaluating modularity in morphometric data: challenges with the RV coefficient and a new test measure. *Methods Ecol. Evol.* **7**, 565–572 (2016).

71. Castiglione, S. et al. A new method for testing evolutionary rate variation and shifts in phenotypic evolution. *Methods Ecol. Evol.* **9**, 974–983 (2018).

Author contributions
The study was conceived by G.S., A.P., S.W. and P.R. D.R.M., S.L., A.P., J.L., M.M. and K.A. processed the endocasts. S.L. and G.S. digitized the landmarks. G.S., P.R., A.P., C.S., S.C., M.M. and A.M. analysed the data. G.S., P.R., A.P. and S.W. wrote the manuscript with substantial contributions from all the other authors.

Competing interests
The authors declare no competing interests.

Additional information
Extended data is available for this paper at https://doi.org/10.1038/s41559-022-01933-6.

Supplementary information The online version contains supplementary material available at https://doi.org/10.1038/s41559-022-01933-6.

Correspondence and requests for materials should be addressed to Gabriele Sansalone or Antonio Profico.

Peer review information *Nature Ecology & Evolution* thanks Amelie Beaudet, Stephen Montgomery and the other, anonymous, reviewer(s) for their contribution to the peer review of this work.
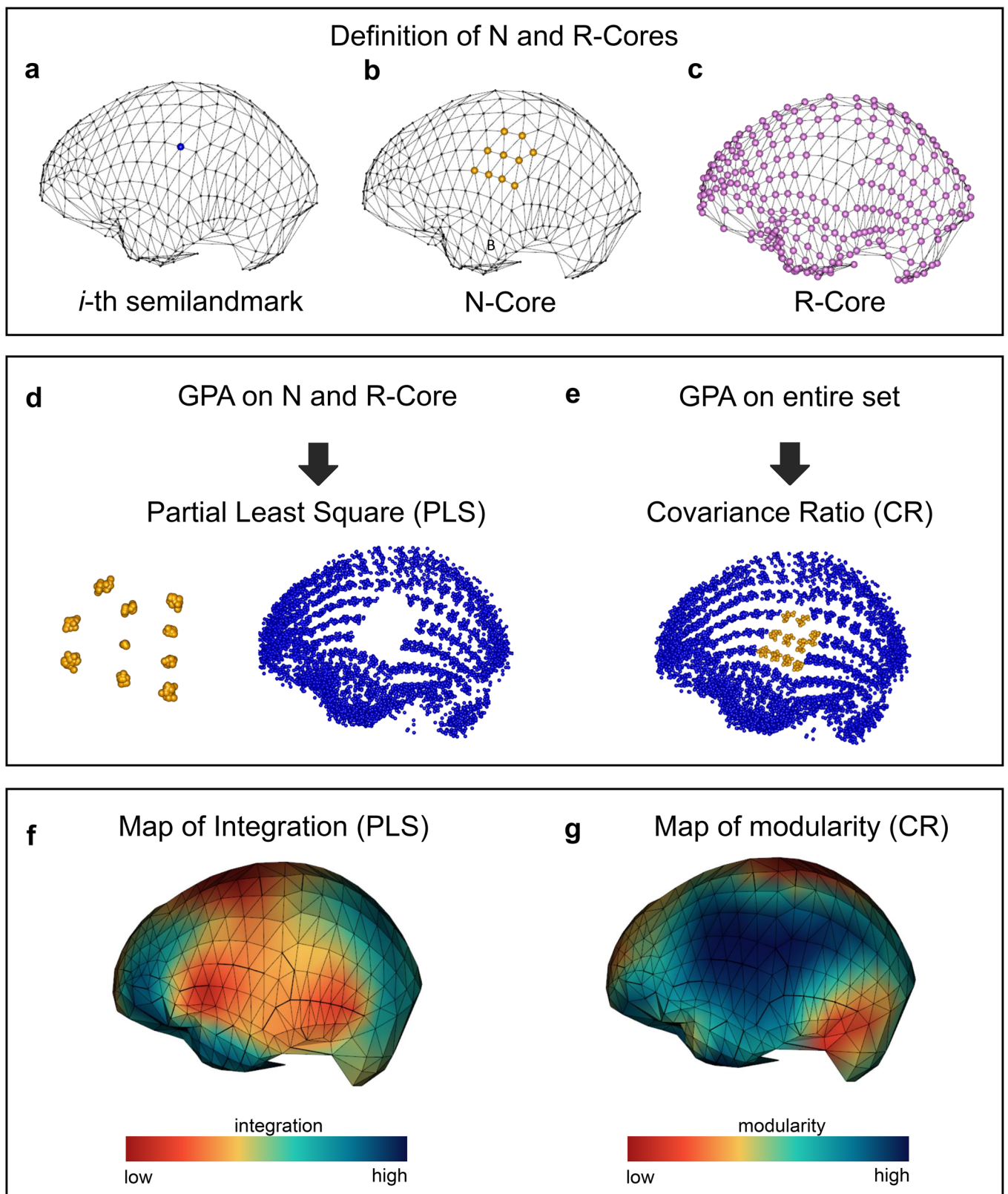
Reprints and permissions information is available at www.nature.com/reprints.

[1]Function, Evolution & Anatomy Research Lab, Zoology Division, School of Environmental and Rural Science, University of New England, Armidale, New South Wales, Australia. [2]Institute for Marine Biological Resources and Biotechnology (IRBIM), National Research Council, Messina, Italy. [3]Department of Biology, University of Pisa, Pisa, Italy. [4]Department of Neuroscience, Washington University School of Medicine, St. Louis, MO, USA. [5]Department of Health Sciences, East Tennessee State University, Johnson City, TN, USA. [6]Department of Archaeology & Palaeoanthropology, School of Humanities, University of New England, Armidale, New South Wales, Australia. [7]College of Science and Engineering, Flinders University, Adelaide, South Australia, Australia. [8]Department of Earth Sciences, Università degli Studi di Firenze, Florence, Italy. [9]Department of Earth Sciences, Environment and Resources, Università degli Studi di Napoli Federico II, Monte Sant'Angelo, Naples, Italy. [10]Research Centre in Evolutionary Anthropology and Palaeoecology, School of Biological and Environmental Sciences, Liverpool John Moores University, Liverpool, UK. [11]These authors contributed equally: Gabriele Sansalone, Antonio Profico. ✉e-mail: gsansalone@uniroma3.it; antonio.profico@gmail.com

Definition of N and R-Cores

a *i*-th semilandmark

b N-Core

c R-Core

d GPA on N and R-Core

Partial Least Square (PLS)

e GPA on entire set

Covariance Ratio (CR)

f Map of Integration (PLS)

integration

low high

g Map of modularity (CR)

modularity

low high

Extended Data Fig. 1 | Endocast local integration assessment. The set of each semilandmark (a) and its 9 closest semilandmarks define the N-Core (b). The remaining semilandmarks define the C-Core (c). The N-Core and R-Core are subjected to two independent GPAs and the covariation between the two blocks is calculated by PLS (d). With CR the GPA is computed the entire set (e). The values from PLS and CR analyses are used to create a colour map of integration (f) and modularity (g).
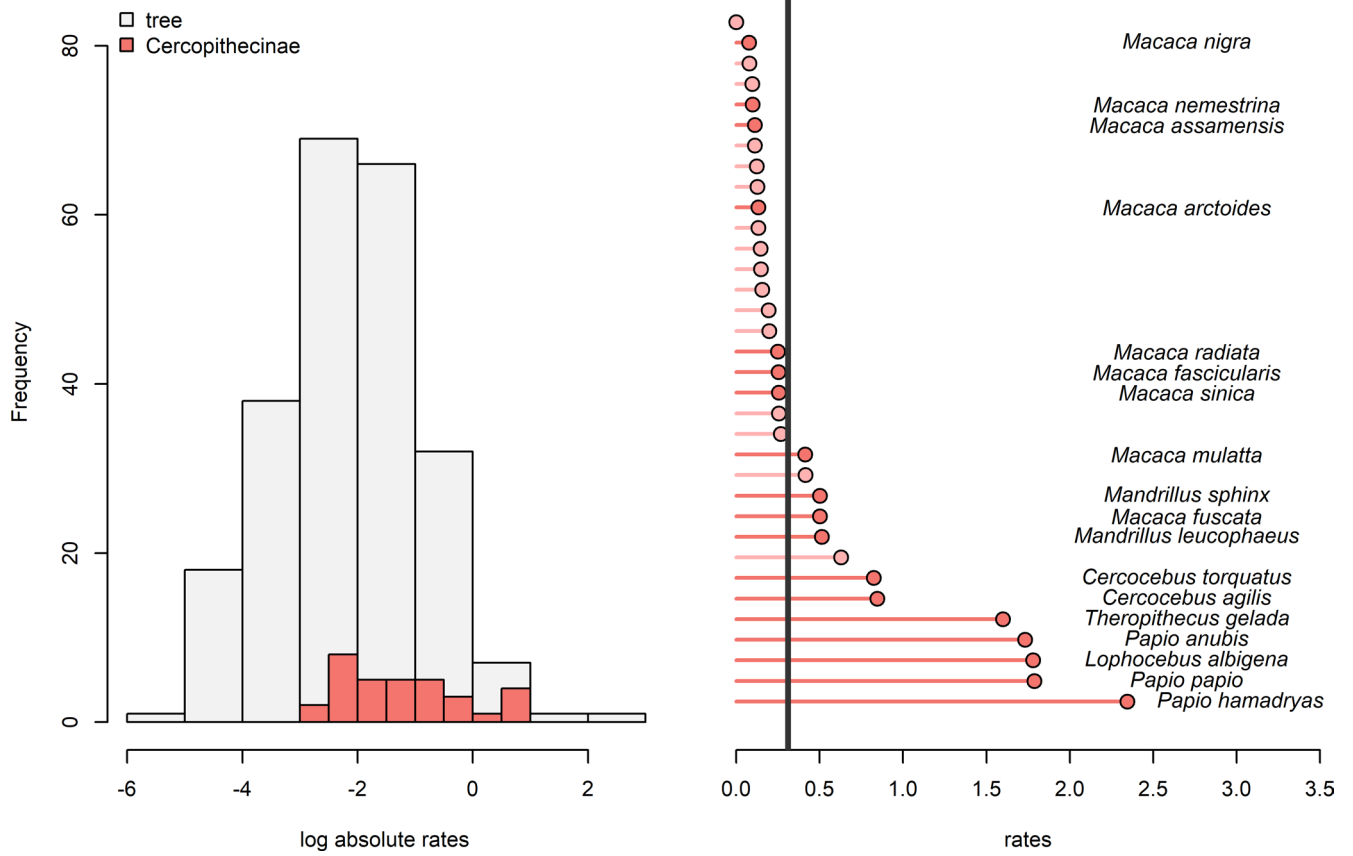
Extended Data Fig. 2 | Evolutionary rates of CR values within the Cercopithecinae clade. Evolutionary rates of CR values within the Cercopithecinae clade.
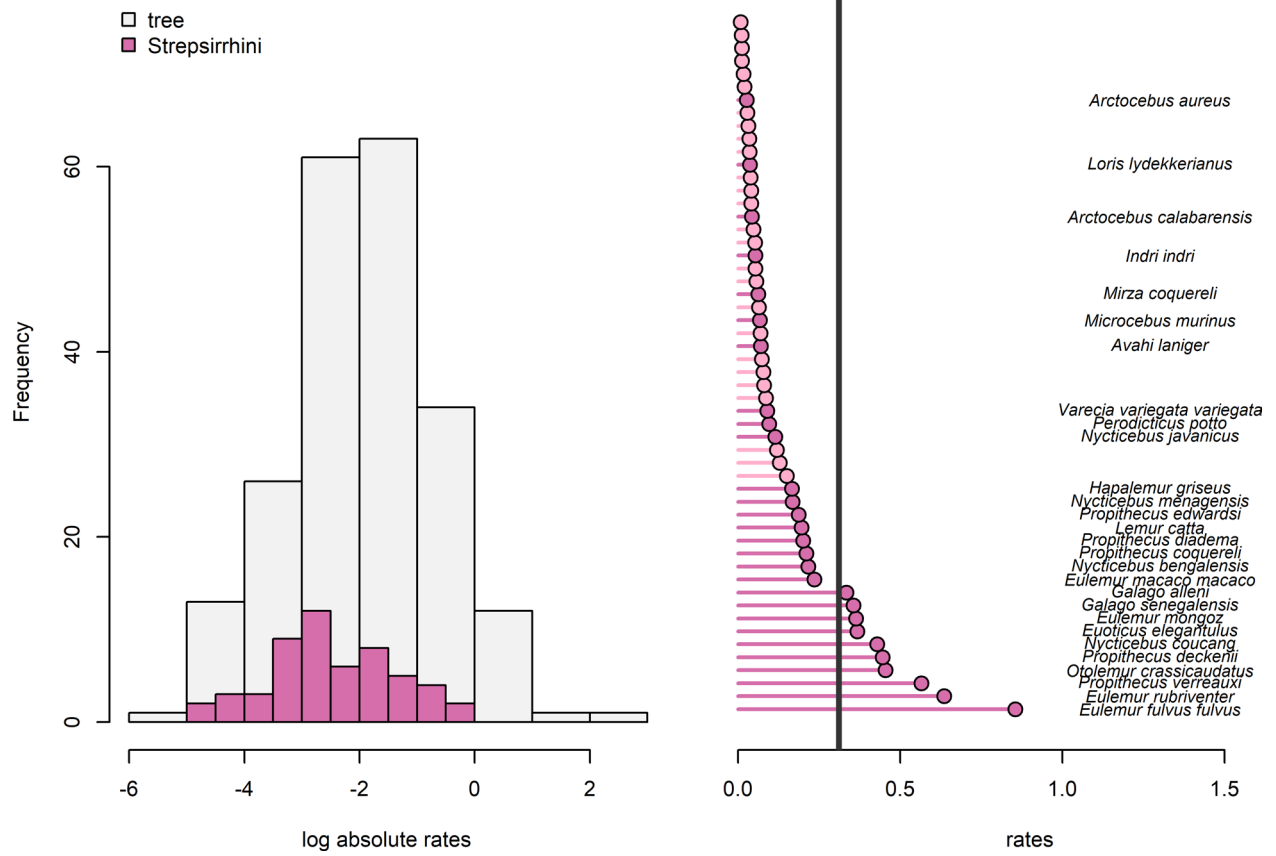
Extended Data Fig. 3 | Evolutionary rates of CR values within the Strepsirrhini. Evolutionary rates of CR values within the Strepsirrhini.

Extended Data Fig. 4 | Evolutionary rates of CR values within the family Cebidae. Evolutionary rates of CR values within the family Cebidae.
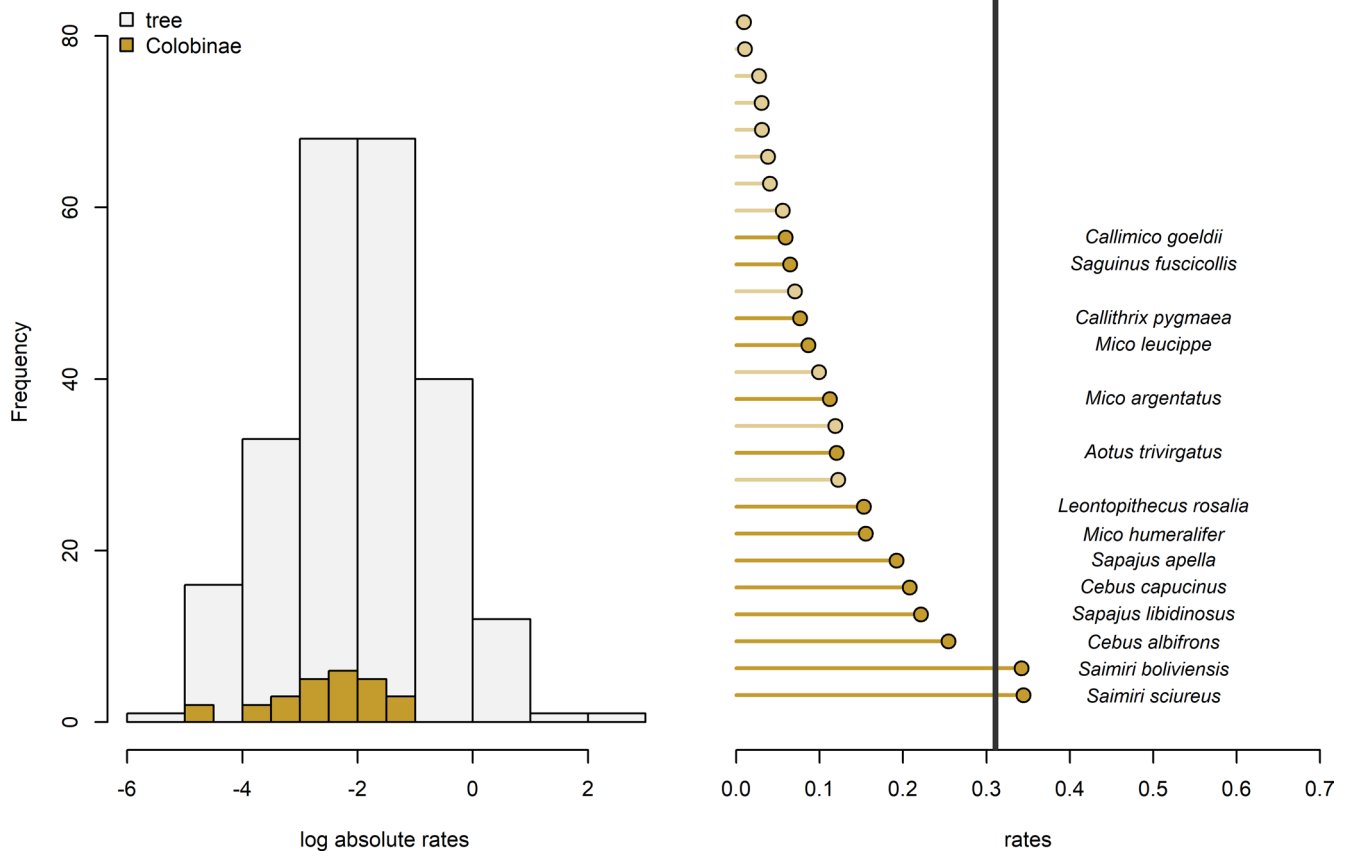
Extended Data Table 1 | R-PLS values

Taxon	Stage 2	Stage 3	Stage 4	Adult
Pan troglodytes	0.93	0.94	0.97	0.57
Homo sapiens	0.91	0.94	0.96	0.93
			Stages 3-4	**Adult**
Gorilla gorilla			0.97	0.71
Pongo sp.			0.94	0.63

R-PLS of separate PLS analyses performed on the different postnatal ontogenetic stages of *H. sapiens*, *P. troglodytes*, *G. gorilla* and *Pongo* species.

Extended Data Table 2 | Effect sizes of separate PLS analyses

Taxon	Stage 2	Stage 3	Stage 4	Adult
Pan troglodytes	0.46	1.33	1.18	0.11
Homo sapiens	1.44	3.77	3.12	2.73
			Stage 3-4	**Adult**
Gorilla gorilla			0.73	0.21
Pongo			1.02	0.17

Effect sizes of separate PLS analyses performed the different postnatal ontogenetic stages of *H. sapiens*, *P. troglodytes*, *G. gorilla* and *Pongo* when accounting for size effect.

Extended Data Table 3 | CR values measured after size and phylogenetic correction

Clade	CR				
Hominoidea	0.963				
Cercopithecinae	0.825				
Colobinae	0.918				
Platyrrhini	0.767				
Strepsirrhini	0.726				

Pairwise test					
	Cercopithecinae	Colobinae	Hominoidea	Platyrrhini	Strepsirrhini
Cercopithecinae		0.468	**<0.001**	**<0.001**	**<0.001**
Colobinae			**<0.001**	**<0.001**	**<0.001**
Hominoidea				**<0.001**	**<0.001**
Platyrrhini					**<0.001**
Strepsirrhini					

Corresponding author(s): Gabriele Sansalone
NATECOLEVOL-220316042C

Last updated by author(s): 26/09/2022

Reporting Summary

Nature Portfolio wishes to improve the reproducibility of the work that we publish. This form provides structure for consistency and transparency in reporting. For further information on Nature Portfolio policies, see our Editorial Policies and the Editorial Policy Checklist.

Statistics

For all statistical analyses, confirm that the following items are present in the figure legend, table legend, main text, or Methods section.

n/a	Confirmed	
☐	☒	The exact sample size (n) for each experimental group/condition, given as a discrete number and unit of measurement
☐	☒	A statement on whether measurements were taken from distinct samples or whether the same sample was measured repeatedly
☐	☒	The statistical test(s) used AND whether they are one- or two-sided *Only common tests should be described solely by name; describe more complex techniques in the Methods section.*
☐	☒	A description of all covariates tested
☐	☒	A description of any assumptions or corrections, such as tests of normality and adjustment for multiple comparisons
☐	☒	A full description of the statistical parameters including central tendency (e.g. means) or other basic estimates (e.g. regression coefficient) AND variation (e.g. standard deviation) or associated estimates of uncertainty (e.g. confidence intervals)
☐	☒	For null hypothesis testing, the test statistic (e.g. F, t, r) with confidence intervals, effect sizes, degrees of freedom and P value noted *Give P values as exact values whenever suitable.*
☒	☐	For Bayesian analysis, information on the choice of priors and Markov chain Monte Carlo settings
☒	☐	For hierarchical and complex designs, identification of the appropriate level for tests and full reporting of outcomes
☐	☒	Estimates of effect sizes (e.g. Cohen's d, Pearson's r), indicating how they were calculated

Our web collection on statistics for biologists contains articles on many of the points above.

Software and code

Policy information about availability of computer code

Data collection	Materialise Mimics v21, Geomagic Studio 2014; IDAV Landmark Editor.
Data analysis	R Statistical software v4.1.3; Morpho v2.9; Geomorph v4.0.3; RRphylo v2.6.0; Arothron v2.0.3. All custom codes and data necessary to replicate the analyses are available in Source codes file.

For manuscripts utilizing custom algorithms or software that are central to the research but not yet described in published literature, software must be made available to editors and reviewers. We strongly encourage code deposition in a community repository (e.g. GitHub). See the Nature Portfolio guidelines for submitting code & software for further information.

Data

Policy information about availability of data

All manuscripts must include a data availability statement. This statement should provide the following information, where applicable:
- Accession codes, unique identifiers, or web links for publicly available datasets
- A description of any restrictions on data availability
- For clinical datasets or third party data, please ensure that the statement adheres to our policy

The authors declare that the data supporting the findings of this study are available within the paper and its supplementary information files. The available data include a time calibrated phylogeny and the aligned Procrustes coordinates for all the considered specimens. Source codes file include the codes necessary to reproduce all the results generated within the manuscript, the codes to reproduce Figures 1, 2 and 3 and all Extended Data Figures.

Field-specific reporting

Please select the one below that is the best fit for your research. If you are not sure, read the appropriate sections before making your selection.

☒ Life sciences ☐ Behavioural & social sciences ☐ Ecological, evolutionary & environmental sciences

For a reference copy of the document with all sections, see nature.com/documents/nr-reporting-summary-flat.pdf

Life sciences study design

All studies must disclose on these points even when the disclosure is negative.

Sample size	Sample size was based to cover the extant primates variability. Sample size of fossil hominins was chosen based on availability, conservation status, and to ensure the broadest phylogenetic sampling. Sample size for ontogenetic stages was chosen to represent the morphological variability of each considered growth stage.
Data exclusions	20 species have been removed to generate the CR values matrix because they were represented only by one specimen.
Replication	Semi-automatic landmarking procedure has been assessed using different templates returning consistent results. Four different modular configurations has been tested and the ost supported one was used in all the analyses. The strategy to measure integration without a priori defined modules has been repeated multiple times to control for consistent results. To account for sampling, phylogenetic uncertainty in tree topology and branch lengths, we used the RRphylo function overfitRR repeated 100 times.
Randomization	Sample was organized into groups based on taxonomic assignment and four growth stages determined by dental eruption timing.
Blinding	Blinding was not possible as all analyses required a priori knowledge of fossil identity in order to accurately reconstruct the endicast morphology.

Reporting for specific materials, systems and methods

We require information from authors about some types of materials, experimental systems and methods used in many studies. Here, indicate whether each material, system or method listed is relevant to your study. If you are not sure if a list item applies to your research, read the appropriate section before selecting a response.

Materials & experimental systems

n/a	Involved in the study
☒	☐ Antibodies
☒	☐ Eukaryotic cell lines
☐	☒ Palaeontology and archaeology
☐	☒ Animals and other organisms
☒	☐ Human research participants
☒	☐ Clinical data
☒	☐ Dual use research of concern

Methods

n/a	Involved in the study
☒	☐ ChIP-seq
☒	☐ Flow cytometry
☒	☐ MRI-based neuroimaging

Palaeontology and Archaeology

Specimen provenance	All specimens used in this study are accessioned into museums with all relevant specimen details. Access to specimen data was granted to the Authors by request to museums and online repositories listed in Supplementary Information. No new specimens were specifically collected as part of this study.
Specimen deposition	All fossils are accessioned. Museums, online repositories and specimen numbers are provided in Supplementary Information.
Dating methods	No new dates are provided. First and last occurrence dates for all species were taken from the literature and provided in Supplementary Information.

☒ Tick this box to confirm that the raw and calibrated dates are available in the paper or in Supplementary Information.

Ethics oversight	No ethical approval or guidance was required for this study.

Note that full information on the approval of the study protocol must also be provided in the manuscript.

Animals and other organisms

Laboratory animals	This study do not involve laboratory animals
Wild animals	No new specimens have been collected for this study.
Field-collected samples	This study do not involve specimens collected in the field.
Ethics oversight	No ethical approval or guidance was required for this study.

Note that full information on the approval of the study protocol must also be provided in the manuscript.